Topographical and geological controls on shallow landslide movement types identified by satellite imagery

YAMAGUCHI, Akari [1]*, SATO, Go [2], Tran The Viet [3], Nguyen Van Thang [3]

[1] First Author's Affiliation: Department of Environmental and Information Studies, Graduate School, Tokyo City University, Japan

[2] Second Author's Affiliation: Department of Environment, Tokyo City University, Japan

[3] Third Author's Affiliation: Faculty of Civil Engineering, Thuyloi University, Vietnam

*g2583023@tcu.ac.jp

Abstract

Extreme rainfall events linked to climate change have increased the frequency of soil disasters in Vietnam. In October 2020, Typhoon Molave triggered thousands of shallow landslides in the southwestern region of Da Nang City. However, the movement processes of landslide debris—such as flow paths and deposition areas–remain poorly understood. This study examined the relationships between topography, geology, and landslide movement types using high-resolution satellite imagery. A total of 7,967 landslides within a 234 km² area were manually classified into four categories: slide-flow (non-channeled), slide-flow (channeled), slide-flow (bed erosion), and slide/fall (non-flow). Their distribution was analyzed with respect to elevation, slope, aspect, and three major geological units (granite, gneiss, and schist). Slide-flow (non-channeled) was the most frequent type (51 %), typically occurring on ridges and upper slopes at elevations of 600–1,000 m with slope angles of 25–35 °. Although less frequent, slide-flow (bed erosion) events produced the largest average landslide areas as debris traveled downslope into valleys. Comparisons among geological units showed that landslides in granite terrain had larger average areas than those in gneiss or schist, likely due to the presence of thick weathered material.

Keywords: Remote sensing, Topographic analysis, Shallow landslides distribution map, Typhoon Molave

1. Introduction

Soil disasters have become increasingly frequent in Vietnam due to extreme rainfall events intensified by climate change [1-4]. Among them, shallow landslides are a major hazard in mountainous regions, threatening human lives, infrastructure, and ecosystems. In October 2020, Typhoon Molave delivered record rainfall to central Vietnam, triggering thousands of shallow landslides in the southwestern part of Da Nang City. This event highlighted the urgent need to better understand the mechanisms controlling landslide initiation and movement under extreme climatic conditions. Previous studies in the region have primarily focused on mapping landslide distribution and assessing susceptibility [5]. While such

approaches provide valuable information on where landslides are likely to occur, they do not adequately explain how displaced material moves downslope, including the flow paths and deposition zones. These processes determine the extent of damage and are critical for hazard assessment and risk management. Therefore, a more detailed classification of landslide movement types is required, integrating both topographical and geological factors. This study aims to clarify the relationships between shallow landslide movement types and topographical and geological conditions in Da Nang City. Using high-resolution satellite imagery, we manually mapped and classified 7,967 landslides triggered by Typhoon Molave into four movement types: slide-flow (non-channeled), slide-flow (channeled), slide-flow (bed erosion), and slide/fall (non-flow) [6]. We then analyzed their distribution in relation to elevation, slope, aspect, and major geological units (granite, gneiss, and schist).

2. Study Area

2.1 Topography

The study area is located in the southwestern part of Da Nang City within the mountainous region that forms part of the Annamite Range (Fig. 1). The Annamite Range formed through orogenic processes associated with the collision between the Indochina and Eurasian plates during the Mesozoic to Cenozoic eras. Subsequent weathering and erosion have resulted in the development of steep mountainous topography [7].

2.2 Geology

The study area comprises three major geological units and five minor ones, grouped due to their limited extent, as indicated in Fig. 2. These units include Cretaceous and Paleogene granite, Proterozoic gneiss, and schist (Table 1). Metamorphic rocks such as gneiss and schist are widely distributed throughout the area, whereas granite intrusions are primarily located in the western part. In this study, we used 1:50,000-scale geological maps published in 2002 by the General Department of Geology and Minerals of Vietnam (GDGMV) [8].

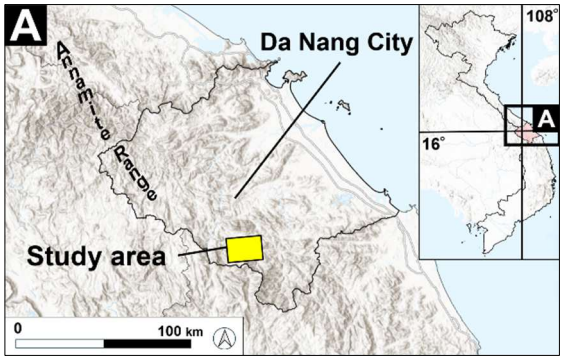

Fig. 1. Topographic map of the study area. This map was made from the 30-m resolution Digital Surface Model (DSM) of ALOS (Daichi).

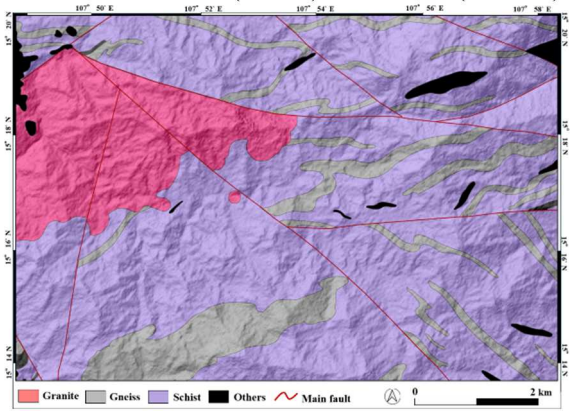

Fig.2. Geology map of the study area. This map was made from 1:50,000 geological map (Phuoc Son, Bac Tra My, Nam Tra My) published by the GDGMV in 2002 [8].

Table 1. Outline of the geology in the study area
(geological age, lithology, geological code, and facies)

Geological time	Rock type	Lithology and Lithofacies
Quaternary	Granite	Phase 2: biotite granite, light color, fine-grained two-mica granite Phase 1: biotite granite, large-grained two-mica granite Dyke phase: aplitic (a) pegmatite (p); quartzite (q); felsite (f); greisen (gr)
Proterozoic	Gneiss	Phase 1: gabbroamphibolite, gabbrodiorite, diorite gneiss Phase 2: tonalite gneiss, granodiorite gneiss, biotite-hornblende gneiss, biotite-hornblende plagiogneiss Amphibole plagiogneiss, amphibole plagioclase-migmatite Biotite gneiss, biotite plagiogneiss, quartz-biotite schist, migmatite Gneiss biotite, plagiogneis biotite, quartz-biotite schist, migmatite Phase 3: plagiogranite gneiss, biotite-amphibole gneiss,
	Schist	High aluminum schist,Quartz-biotite-sillimanite schist, quartz-plagioclas-biotite-sillimanite-garnet schist, twmica-quartz-sillimanite schist Quartz-biotite-schist, biotite plagiogneiss intercalated High aluminum schist, quartz-plagioclase-biotite-sillimanite-garnet schist, quartz-plagioclase-biotite-sillimanite- schist

3. Classification of landslide movement types

3.1 Landslide morphometric mapping

Topographic interpretation was conducted using satellite imagery (Google Earth) to classify landslides by movement type. This study used satellite images captured after the heavy rainfall on October 1, 2021. Although the acquisition time and resolution of the satellite images varied depending on location, the images of the study area provided sufficient accuracy for interpreting landslide sites. These high-resolution images offered detailed visual information on terrain characteristics and the precise locations of landslides. Landslide polygons were delineated using the polygon drawing tool in Google Earth. Figure 2 (A–C) presents satellite images taken before and after the landslides, along with the distribution of landslides classified by movement type. The polygons delineating the landslide areas were not separated into source and deposition zones. Instead, both landforms were treated as a single landslide area (Fig. 2B). Specific points were also identified as landslide sources (Fig. 2C). All landslides were manually classified according to movement type. Following the classification scheme of Hao Ma et al. (2024), landslides were categorized into four types: Slide-flow (non-channeled), as shown in Fig. 3-I, Slide-flow (channeled) in Fig. 3-II, Slide-flow (bed erosion) in Fig. 3-III, and Slide/Fall (non-flow) in Fig. 3-IV (summarized in Fig. 3-V). As shown in Table 2, the classification was based on landslide topography, occurrence of flow, presence of channels, and extent of the deposition area.

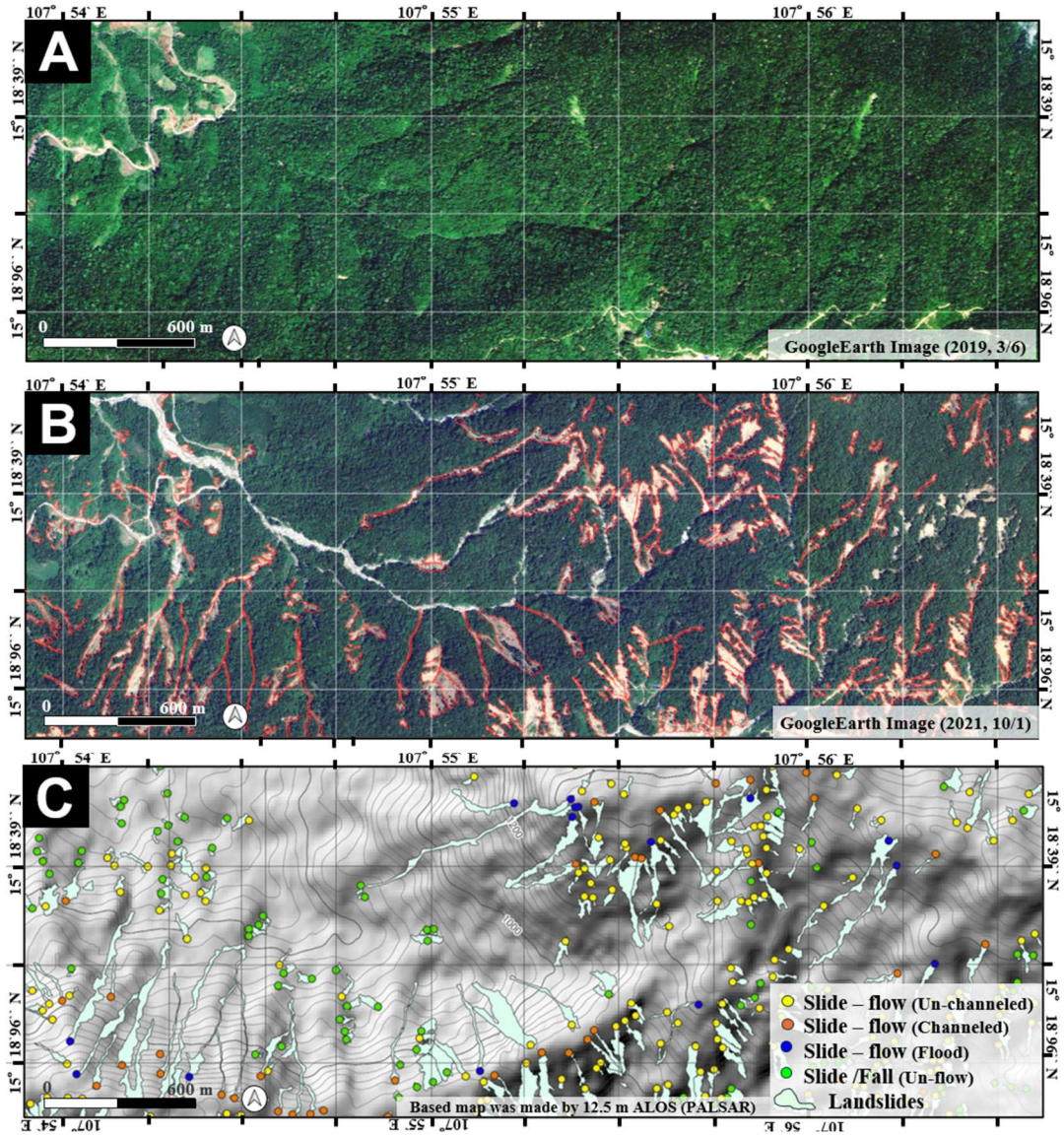

Fig. 2. A) Satellite image before landslide occurrence, captured on March 6, 2019. This map was made using Google Earth satellite imagery. B) Satellite image after landslide occurrence, captured on October 1, 2021. This map was made using Google Earth satellite imagery. C) Distribution of landslides classified by movement type. This map was made from the 30-m resolution Digital Surface Model (DSM) of ALOS (PALSAR).

Table 2. Typical characteristics for identifying landslide movement types

Movement types of landslide	Description
Slide-flow (non-channeled)	The landslide mass moves without being constrained by valley morphology.
Slide-flow (channeled)	The landslide mass moves while constrained by the valleys. Channels' morphology.
Slide-flow (bed erosion)	The landslide mass becomes fluidized and travels downslope while eroding the slope bed.
Slide/Fall (non-flow)	No apparent fluidization is observed in the landslide mass. This type primarily corresponds to small-scale slides or rockfalls.

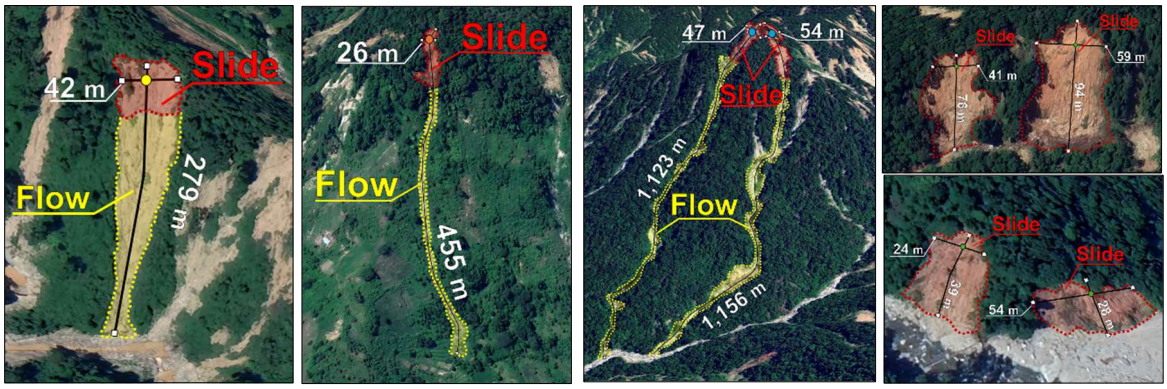

Fig.3. Fig. 3. Typical features of landslide movement types identified in satellite imagery. This map was made from Google Earth imagery captured on October 1, 2021.

3.2 Distribution of landslides and characteristics of landslide area by Movement types

Figure 4 shows the distribution of shallow landslides induced by heavy rainfall in October 2020 on a topographical map of the study area. Figure 5 shows the distribution of landslides classified by movement type; 7,967 landslide sites were manually identified within the 234 km² study area. Table 3 presents the number of landslides by movement type and the average landslide area. In terms of the number of landslides, slide flow (non-channeled) accounted for 4,076 cases, slide fall (non-flow) for 3,078, slide flow (channeled) for 621, and slide flow (bed erosion) for 192. Regarding the average landslide area, slide flow (bed erosion) recorded the largest value at 8,909.1 m², followed by slide flow (channeled) at 3,753.9 m². The proportion of slide flow landslides per unit area by movement type is as follows. For slide flow (non-channeled), the largest proportion was 24.3 % in the 500–1,000 m² class, followed by 16.9 % in the 1,000–1,500 m² class. For slide flow (channeled), 23.2 % occurred in areas larger than 5,000 m², followed by 11.9 % in the 1,500–2,000 m² class. For slide flow (bed erosion), 67.4 % occurred in areas larger than 5,000 m², followed by 7.9 % in the 3,500–4,000 m² class. For slide fall (non-flow), 47.5 % occurred in the 0–500 m² class, followed by 25.1 % in the 500–1,000 m² class. These results indicate that the most frequent movement type in the study area was slide flow (non-channeled), with 4,076 occurrences, accounting for 51.2 % of the total. Many steep slopes without well-developed valley topography were present in the study area. Consequently, the debris generated by slope failures tended to move and deposit on slopes without being constrained by specific valleys. Therefore, several slide flow (non-channeled) landslides were observed in the study area. In addition, the number of slide/fall (unflow) landslides was 3,078, accounting for 38.6 % of the total. This movement type is characterized by the short travel distance of landslide debris without fluidization, and the average landslide area (910.5 m²) was smaller than that of other movement types. Interpretation of satellite

imagery confirmed that many of these landslides occurred along roads and in the vicinity of residential areas. Therefore, although the average landslide area was relatively small, they represent a movement type with a high risk of causing damage to humans and property. In contrast, slide flow (channeled) and slide flow (bed erosion) landslides were fewer in number but exhibited larger average landslide areas. In particular, slide flow (bed erosion) accounted for approximately 70 % of large-scale landslides exceeding 5,000 m². Although their occurrence was localized, the landslide mass was substantial and reached downstream areas.

Table 3. Number and total area of landslide movement types represented in the inventory map

	Slide-flow (non-channeled)	Slide-flow (channeled)	Slide-flow (bed erosion)	Slide/fall (non-flow)
Number of landslides	4,076	621	192	3,078
Proportion of landslide (%)	51.2	7.8	2.4	38.6
Average landslide area (m^2)	1,936.8	3,753.9	8,909.1	910.5

Table 4. Number and proportional distribution of landslides by movement types and area classes

Landslide area (m^2)	Number of landslides				Proportion of landslide (%)			
	Non-channeled	Channeled	Bed erosion	Non-flow	Non-channeled	Channeled	Bed erosion	Non-flow
0~500	648	26	0	1,432	16.0	4.3	0	47.5
500~1,000	983	50	4	756	24.3	8.2	2.1	25.1
1,000~1,500	682	66	4	343	16.9	10.8	2.1	11.4
1,500~2,000	481	73	8	162	11.9	11.9	4.2	5.4
2,000~2,500	312	60	5	91	7.7	9.8	2.6	3.0
2,500~3,000	224	49	6	82	5.5	8.0	3.2	2.7
3,000~3,500	177	42	2	39	4.4	6.9	1.1	1.3
3,500~4,000	102	38	15	27	2.5	6.2	7.9	0.9
4,000~4,500	87	41	9	20	2.2	6.7	4.7	0.7
4,500~5,000	70	24	9	17	1.7	3.9	4.7	0.6
5,000≧	278	142	128	43	6.9	23.2	67.4	1.4

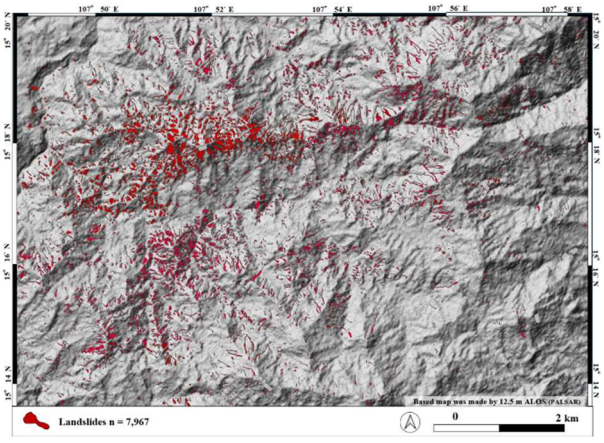

Fig.4. Topography map of the study area showing the distribution of shallow landslides induced by heavy rain in October 2020. This map was made from a 12.5 m DSM derived from ALOS (PALSAR)

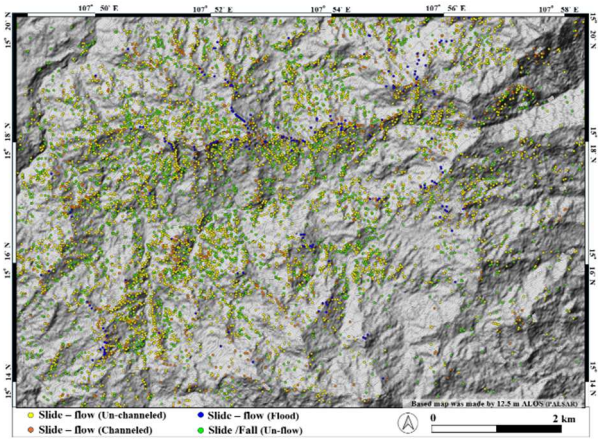

Fig.5. Distribution of landslides classified based on movement type. This map was made from a 12.5 m DSM derived from ALOS (PALSAR)

4. Relationship between landslide and topographical and geological conditions

4.1 Topography and geology analysis

Topographic analysis was conducted for the landslide source areas to identify the topographical characteristics of each movement type. This study employed three topographical parameters—elevation, slope angle, and slope aspect—as summarized in Table 5. Figures 6A–6C show the distribution of landslides classified according to movement type based on each topographic parameter. These topographical datasets were generated from a 12.5-m resolution DSM derived from ALOS (PALSAR) data. The analysis was performed using QGIS (version 3.30). Subsequently, to clarify the relationship between landslide movement type and geology, a comparative analysis was conducted for the three main geological units: granite, gneiss, and schist (Table 1). The distribution of landslides by movement type and average landslide area were compared. Figure 6D shows the distribution of landslides classified by movement type on a geological map.

Table 5. Classification and structure of parameters used for topographic analysis

Factors	Class	Description
Elevation (m)	0~200, 200~400, 400~600, 600~800, 800~1,000, 1,000~1,200, 1,200~1,400, 1,400~1,600, 1,600~1,800, 1,800~2,000	Elevation values are divided into 200 m intervals.
Slope (°)	0–5, 5–10, 10–15, 15–20, 20–25, 25–30, 30–35, 35–40, 40–45, 45–50, 50–55, 55–60, 60–65	Slope angle is divided into a 5° interval.
Aspect	N–North, NE–Northeast, E–East, SE–Southeast, S–South, SW–Southwest, W–West, NW–Northwest, F–Flat (no dominant aspect)	Aspect is categorized into 8 cardinal and intercardinal directions.

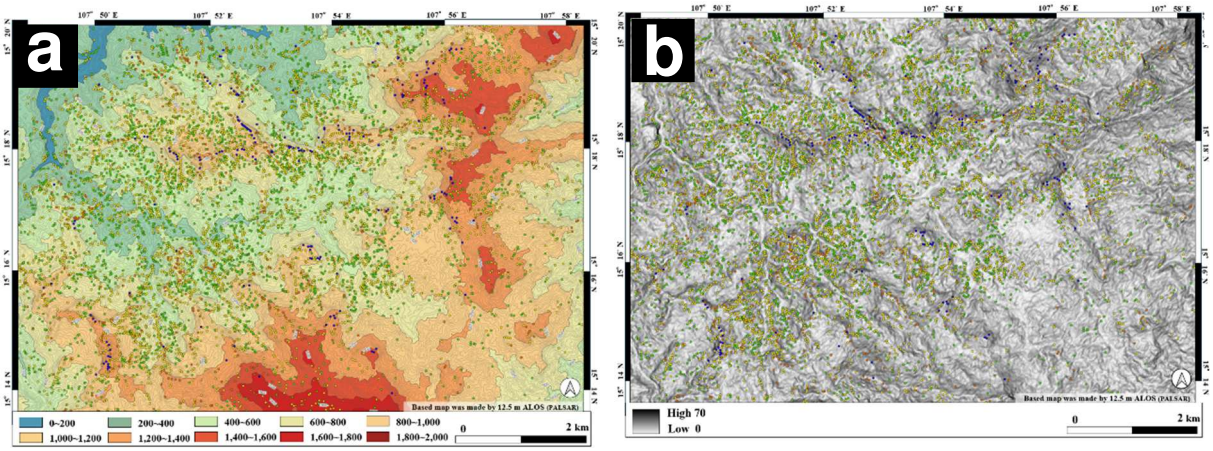

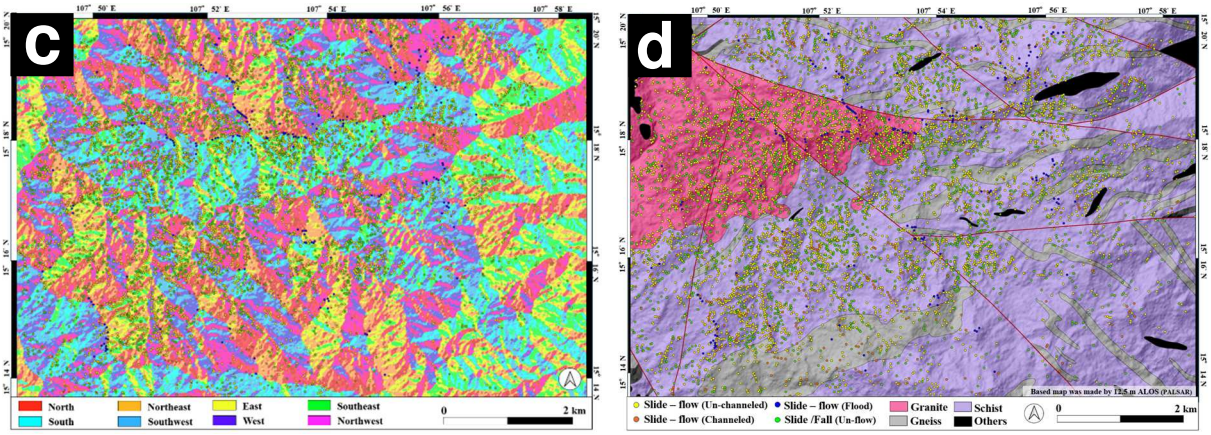

Fig.6. Distribution of landslides classified by movement types based on each factor: (a) Elevation, (b) Slope, (c) Slope aspect, (d) Geology. (a–c) were made from a 12.5 m DSM derived from ALOS (PALSAR). Map (d) was made from a 1:50,000 geological map published by the GDGMV in 2002.

4.2 Topography characteristics of landslides by movement types

Tables 6–8 and Figure 7 present the proportion of landslides by movement type, classified according to each topographical parameter. Based on these results, the geomorphological characteristics of each movement type were summarized. The following trends were identified: Slide-flow (non-channeled) landslides were concentrated at elevations of 600–1,000 m, on slopes of 20–30°, with north–northeast aspects, and many of their landslide sources were located on ridges and middle slopes. Slide-flow (channeled) landslides were concentrated at elevations of 800–1,200 m, on slopes of 15–30°, with north–northeast aspects, and many of their landslide sources were located on ridges and middle slopes. Slide-flow (bed erosion) landslides were concentrated at elevations of 1,000–1,400 m, on slopes of 20–35°, with northwest–north aspects, and many of their landslide sources were located on ridges and middle slopes. Slide/fall (non-flow) landslides were concentrated at elevations of 600–1,000 m, on slopes of 15–25°, with north aspects, and many of their landslide sources were located on the middle and lower slopes. From these results, slide-flow (non-channeled) landslides were concentrated in lower elevations and middle slopes compared to other flow-type landslides. In contrast, slide-flow (channeled) and slide-flow (bed erosion) landslides were concentrated at higher elevations and on steep ridge slopes, where the landslide sources were located. Accordingly, the mass generated by these landslides was considered to have moved downslope along the valley topography from the steep ridge areas. Compared to other movement types, slide/fall (non-flow) landslides were concentrated on gentle slopes, lower to middle slopes, and valleys where their landslide sources were located. Therefore, a landslide mass of this type was considered limited to the initial stage, resulting in short runout distances or in-place deposition.

Table 6. Topographic analysis results showing the proportion of landslides by movement types according to elevation classes.

Elevation (m)	0~200	200~400	400~600	600~800	800~1,000	1,000~1,200	1,200~1,400	1,400~1,600	1,600~1,800	1,800~2,000
Non-channeled	0	0.4	8.6	25.6	29.3	21.1	12.0	2.2	0.7	0
Channeled	0	0	4.2	18.7	24.3	26.4	18.5	5.6	1.8	0.5
Bed erosion	0	0	2.1	4.1	19.2	36.3	26.9	9.8	1.0	0.5
Non-flow	0	1.0	14.3	31.6	31.1	15.0	5.3	1.6	0.2	0

Table 7. Topographic analysis results showing the proportion of landslides by movement types according to slope classes.

Slope (°)	0~5	5~10	10~15	15~20	20~25	25~30	30~35	35~40	40~45	45~50	50~55	55~60	60~65
Non-channeled	1.3	4.3	9.7	16.0	19.0	21.4	15.2	8.1	3.5	1.1	0.4	0	0
Channeled	1.0	5.1	11.3	16.9	16.7	17.5	15.4	10.5	3.4	2.1	0.2	0	0
Bed erosion	2.1	6.3	9.4	16.1	16.7	14.6	16.7	8.9	5.2	3.1	1.0	0	0
Non-flow	1.6	6.5	13.5	19.6	21.6	18.6	11.1	5.2	1.8	0.5	0	0	0

Table 8. Topographic analysis results showing the proportion of landslides by movement types according to slope aspect classes.

Aspect	N 337.5~22.5	NE ~67.5	E ~112.5	SE ~157.5	S ~202.5	SW ~247.5	W ~292.5	NW ~337.5
Non-channeled	13.3	14.1	12.5	13.2	12.8	11.8	10.2	12.2
Channeled	18.7	16.9	8.9	10.3	11.9	9.5	11.1	12.7
Bed erosion	15.5	13.0	8.8	8.3	13.0	9.8	13.5	18.1
Non-flow	14.0	12.5	12.7	12.7	12.2	12.7	11.2	11.9

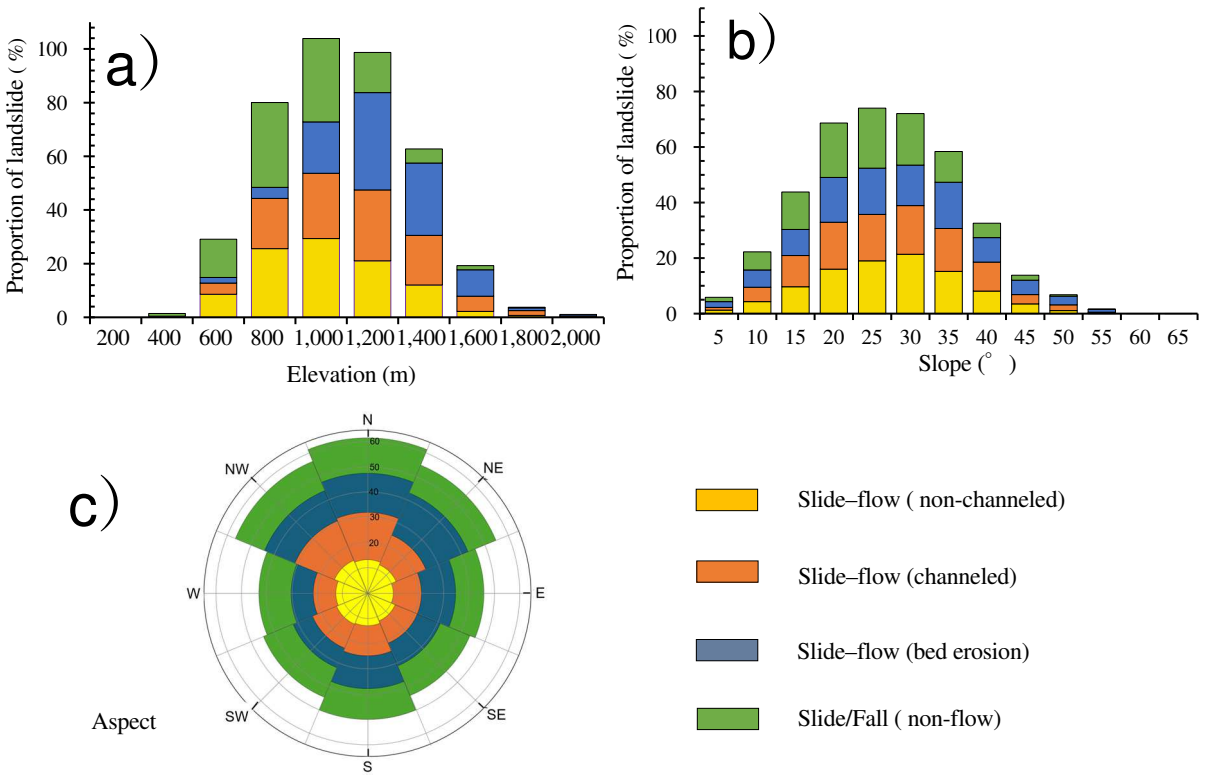

Fig. 7. Initial landslide sites using four basic topographical parameters. a) Elevation, b) Slope, c) Slope aspect

5. Relationship between landslide movement types and geology

In this study, comparisons were made between the distribution of landslides and the average landslide area for each movement type across the main geological units of the study area: granite, gneiss, and schist. Figure 8 shows the distribution of landslides classified by movement type superimposed on a geological map. From the average landslide area by movement type for each geological unit shown in Table 9, in the granite area, the average landslide area was 2,310.2 m² for slide-flow (non-channeled), 4,999.1 m² for slide-flow (channeled), 9,915.1 m² for slide-flow (bed erosion), and 1,263.0 m² for slide/fall (non-flow). In the gneiss area, the average landslide area was 1,606.1 m² for slide-flow (non-channeled), 4,317.4 m² for slide-flow (channeled), 11,798.7 m² for slide-flow (bed erosion), and 858.2 m² for slide/fall (non-flow). In the schist area, the average landslide area was 1,841.8 m² for slide-flow (non-channeled), 3,264.6 m² for slide-flow (channeled), 8,102.5 m² for slide-flow (bed erosion), and 758.3 m² for slide/fall (non-flow). These results indicate that the average landslide area in the granite zone was larger than in the gneiss and schist zones for all movement types, except for slide-flow (bed erosion). This tendency was particularly remarkable for the slide/fall (non-flow) type. In the study area, under the Asian monsoon climate, granite is highly weathered, forming a thick decomposed layer [9]. Decomposed granite is further exposed at the surface and rapidly weathers, making it more susceptible to failure during heavy rainfall [10]. In addition, a thick weathered zone composed of decomposed granite is thought to have facilitated rainfall infiltration, which increased the pore water pressure at the boundary with the bedrock, thereby triggering large-scale landslides. The proportions of landslides by movement type for each geological unit are shown in Figure 9 and Table 10. In the granite area, the proportion of landslides was 49.9 % for slide-flow (non-channeled), 5.8 % for slide-flow (channeled), 2.7 % for slide-flow (bed erosion), and 41.6 % for slide/fall (non-flow). In the gneiss area, the proportion of landslides was 59.2 % for slide-flow (non-channeled), 11.0 % for slide-flow (channeled), 1.8 % for slide-flow (bed erosion), and 27.9 % for slide/fall (non-flow). In the schist area, the proportion of landslides was 50.5 % for slide-flow (non-channeled), 8.1 % for slide-flow (channeled), 2.4 % for slide-flow (bed erosion), and 39.0 % for slide/fall (non-flow). These results indicate that the proportion of landslides by movement type showed a similar trend across all geological units. However, as listed in Table 9, even for the same movement type, the average landslide area differed depending on the geological unit.

Table 9. Average landslide area by movement types for each geological unit.

Landslide types	Granite	Gneiss	Schist
Slide-flow (non-channeled)	2,310.2	1,606.1	1,841.8
Slide-flow (channeled)	4,999.1	4,317.4	3,264.6
Slide-flow (bed erosion)	9,915.1	11,798.7	8,102.5
Slide/Fall (non-flow)	1,263.3	858.2	758.3

Table 10. Number and proportion of landslides by movement types for each geological unit

Landslide types	Granite	Gneiss	Schist
Slide-flow (non-channeled)	1,040 (49.9)	452 (59.2)	2,583 (50.5)
Slide-flow (channeled)	121 (5.8)	84 (11.0)	416 (8.1)
Slide-flow (bed erosion)	56 (2.7)	14 (1.8)	122 (2.4)
Slide/Fall (non-flow)	868 (41.6)	213 (27.9)	1,997 (39.0)

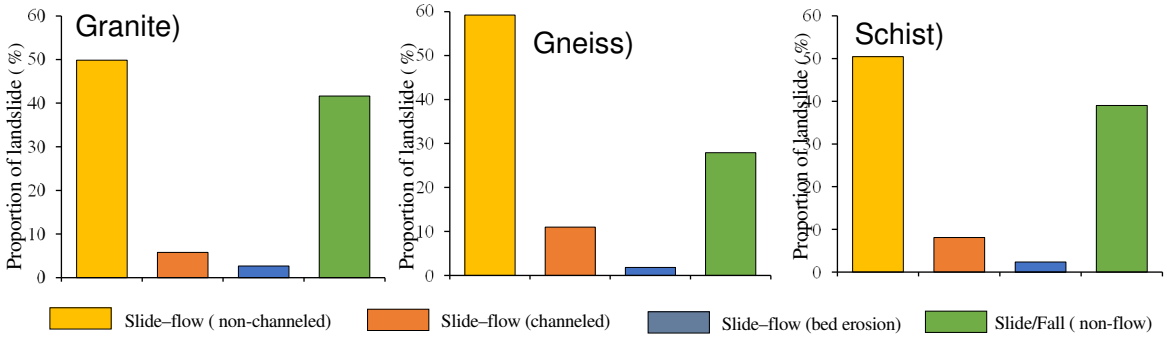

Fig.9. Proportion of the number of landslides by movement types for each geological unit

Conclusion

In this study, topographic interpretation using satellite imagery was conducted, and landslide movement types were classified by distinguishing between the landslide source and deposition areas. Furthermore, the relationships between the landslide movement types and topographical and geological characteristics were examined. Consequently, the following findings were obtained.

1） Distribution of landslides and characteristics of landslide areas by movement types

The results revealed 7,967 landslides were identified within 234 km² of the study area. The most frequent movement type was slide-flow (non-channeled), accounting for approximately 51 % of the total. This dominance can be attributed to the prevalence of steep slopes without well-developed valley topography, where slope-failure debris tends to move and deposit on slopes without being constrained by specific valleys. Slide/fall (unflow) accounted for approximately 39 % of the total. Although this type is generally smaller in scale, many cases have been identified along roads and near residential areas, indicating a

relatively high risk of human and property damage. In contrast, slide-flows (channeled) and slide-flows (bed erosion) occurred less frequently but exhibited larger average landslide areas. In particular, Slide-flow (bed erosion) accounts for approximately 70 % of large-scale landslides exceeding 5,000 m², and the landslide mass frequently reaches downstream areas.

2）Topographic characteristics of landslides by movement type

Slide-flow (non-channeled) landslides were mainly distributed on middle slopes at elevations of 600–1,000 m, concentrated on steep slopes of 25–35°. Slide-flow (channeled) landslides occurred frequently along ridges and valleys at elevations of 800–1,200 m, and were concentrated on slopes steeper than 30°. Slide-flow (bed erosion) landslides were concentrated on steep ridges above 1,000 m, showing the characteristics of scouring valley floors as the landslide debris flowed downstream. Slide-fall (non-flow) landslides were mainly distributed on gentle to moderate slopes at elevations of 600–1,000 m, concentrated on slopes of 20–30°. Regarding slope aspect, all movement types were relatively more frequent on northwest-to-northeast-facing slopes, suggesting the influence of localized rainfall and topographic conditions. These results indicate that each movement type exhibits a characteristic distribution pattern depending on elevation, slope angle, and slope aspect.

3) Relationship between landslide movement types and geology

The results show that the proportion of landslide occurrences by movement type exhibited no remarkable differences among the three main geological units (granite, gneiss, and schist). However, the granite area exhibited a larger average landslide area than other geological units. This tendency was particularly evident for slides and falls (unflowing). The granite area is characterized by a thick weathered zone composed of decomposed granite. Rainfall infiltration into this weathered layer is considered to have increased the pore water pressure at the boundary with the underlying bedrock, thereby triggering large-scale landslides.

References

1. Bui, T.D., Tran, A.T., Hoang, D.N., Nguyen, Q.T., Nguyen, B.D., Ngo, V.L., and Pradhan, B. (2017). Spatial prediction of rainfall-induced landslides for the Lao Cai area (Vietnam) using a hybrid intelligent approach of least squares support vector machines inference model and artificial bee colony optimization. Landslides, 14: 447–458.
2. Tran, T.V., Alvioli, M., Lee, G.H., and An, H. (2018). Three-dimensional, time-dependent modeling of rainfall-induced landslides over a digital landscape: a case study. Landslides, 15: 1071–1084.

3. Nguyen, V.T., Wakai, A., Sato, G., Tran, T.T., and Nanaha, K. (2022). Simple method for shallow landslide prediction based on wide-area terrain analysis incorporated with surface and subsurface flows. Natural Hazards Review, 23(4): 1–17.
4. Tran, T.V., Thu, T.M., Lee, G.H., Oh, S., and Van, N.T.H. (2015). Effect of extreme rainfall on cut slope stability: A case study in Yen Bai City, Vietnam. Journal of the Korean Geo-Environmental Society, 16(4): 23–32.
5. Yamaguchi, A., Sato, G., Tran, T.V., Nguyen, V.T., and Ozaki, T. (2025). Evaluating landslide dimensions and distribution across different geological settings in Quang Nam Province following Typhoon Molave. Proceedings of the 5th ICSCE, Vol. 2.
6. Ma, H., and Wang, F. (2024). Inventory of shallow landslides triggered by extreme precipitation in July 2023 in Beijing, China. Scientific Data, 11.
7. Coudrat, C.N.Z. (2022). The Annamite Mountains – A Biodiverse Ecosystem at Risk: A Case Study in Nakai–Nam Theun National Park, Lao P.D.R. In: Imperiled: The Encyclopedia of Conservation, pp. 583–596.
8. General Department of Geology and Minerals of Vietnam (GDGMV). (2002). Geological and Mineral Map at 1:50,000 scale of the Lào Cai sheet group, including sheets: Phuoc Son (F-49-123-A), Bac Tra My (F-49-123-B), Nam Tra My (F-49-123-C).
9. Tran, A.T., Tran, T.T., and Pham, X. (2023). Landslide susceptibility mapping based on the weights of evidence model for mountainous areas of Quang Nam Province, Vietnam. Hydrol-Meteorology, pp. 31–45.
10. Chigira, M. (1998). Introduction to Disaster Geology. Kinmiraisha, pp. 22–23. (in Japanese).